arXiv:hep-ex/0106048v1 12 Jun 2001

Study of the $\pi\pi$ mass spectra in the process $e^+e^- \to \pi^+\pi^-\pi^0$ at $\sqrt{s} \simeq 1020$ MeV.

M.N.Achasov*, V.M.Aulchenko, K.I.Beloborodov,
A.V.Berdyugin,A.G.Bogdanchikov, A.V.Bozhenok, A.D.Bukin, D.A.Bukin,
S.V.Burdin, T.V.Dimova, V.P.Druzhinin, V.B.Golubev, V.N.Ivanchenko,
P.M.Ivanov, A.A.Korol, M.S.Korostelev, S.V.Koshuba, A.V.Otboev,
E.V.Pakhtusova, E.A.Perevedentsev, A.A.Salnikov, S.I.Serednyakov, V.V.Shary,
Yu.M.Shatunov, V.A.Sidorov, Z.K.Silagadze, A.V.Vasiljev, Yu.S.Velikzhanin
Budker Institute of Nuclear Physics,
Siberian Branch of the Russian Academy of Sciences and
Novosibirsk State University,
11 Laurentyev,Novosibirsk,
630090, Russia

The invariant mass spectra of the $\pi^+\pi^-$ and $\pi^\pm\pi^0$ pairs in the process $e^+e^- \to \pi^+\pi^-\pi^0$ were studied in the SND experiment at the VEPP-2M collider in the energy region $\sqrt{s} \simeq 1020$ MeV. These studies were based on about 0.5×10^6 experimental events. The spectra were analyzed in the framework of the vector meson dominance model. It was found that the experimental data can be described with $e^+e^- \to \rho\pi \to \pi^+\pi^-\pi^0$ transition only. Upper limit on the branching ratio of the $\phi(1020) \to \pi^+\pi^-\pi^0$ decay through intermediate states different from $\rho\pi$ was obtained at the 90 % confidence level: $B(\phi \to \pi^+\pi^-\pi^0) < 6 \cdot 10^{-4}$. The ρ-meson mass and width which follow from the spectra analysis are $m_\rho = 775.0 \pm 1.3$ MeV, $\Gamma_\rho = 150.4 \pm 3.0$ MeV. Neutral and charged ρ-mesons mass difference was found to equal $m_{\rho^\pm} - m_{\rho^0} = -1.3 \pm 2.3$ MeV. In the $\pi^+\pi^-$ mass spectrum the $\rho - \omega$ interference was seen at two standard deviations level.

I. INTRODUCTION

In the framework of the vector meson dominance model (VDM) the cross section of the process $e^+e^- \to \pi^+\pi^-\pi^0$ in the energy region $\sqrt{s} \sim 1$ GeV is determined by the amplitudes of vector mesons V ($V = \omega, \phi, \omega', \omega''$) transitions into the final state: $V \to \pi^+\pi^-\pi^0$. From experimental data it is known that the $\rho\pi$ intermediate state dominates in these transitions. In the energy region $\sqrt{s} \simeq m_\phi$ the main contribution to the cross section comes from the $\phi(1020)$-meson decay $\phi \to \rho\pi \to \pi^+\pi^-\pi^0$. The total cross section of the process $e^+e^- \to \pi^+\pi^-\pi^0$ in the vicinity of the $\phi(1020)$ resonance was studied in several experiments[1−6], including the SND (Spherical Neutral Detector) experiment at VEPP-2M collider[7]. Studies of this process dynamics (the dipion mass distribution) were reported only in two works[6,8].

The transition $V \to \pi^+\pi^-\pi^0$ besides $\rho\pi$ intermediate state (Fig.1a) can be performed by $\rho'^{('')}\pi$ intermediate state (Fig.1c). Even if the branching ratio of the $V \to \rho'^{('')}\pi$ decay is rather small, the interference of this amplitude with the $V \to \rho\pi$ amplitude can give the noticeable contribution to the total cross section. The transition $e^+e^- \to \pi^+\pi^-\pi^0$ is also possible through $\rho - \omega$ interference: $e^+e^- \to V \to \omega\pi^0 \to \rho^0\pi^0$ ($V = \rho, \rho', \rho''$) (Fig.1b). This effect was observed

---

[*] E-mail: achasov@inp.nsk.su, FAX: +7(383-2)34-21-63

in the SND experiment in the energy region $\sqrt{s} = 1200$–1400 MeV[9]. In the process $e^+e^- \to \rho\pi$ the interaction of the ρ-meson with pion in the final state is also expected[10] (Fig.1d).

Besides of the $V \to 3\pi$ transition dynamics studies, the process $e^+e^- \to \pi^+\pi^-\pi^0$ in the $\phi(1020)$ resonance energy region can be used for the ρ-meson parameters measurement. In the reaction $e^+e^- \to \rho\pi$ the neutral and charged ρ-mesons are produced, so it can be used for the $\rho^\pm$ and ρ^0 mass difference determination[11]. The ρ mass values obtained by using different reactions contradict to each other[12]. So it is worthwhile to compare the resonance parameters (m_ρ and Γ_ρ), obtained from the $e^+e^- \to \rho\pi$ reaction with the results of other experiments.

Investigation of the $\pi\pi$ mass distribution in the process $e^+e^- \to \pi^+\pi^-\pi^0$ provides important information about vector mesons and their interference. Here we present the results of the dipion mass spectra analysis in SND experiment.

II. DATA ANALYSIS

A. Experiment

The SND detector[13] operated since 1995 up to 2000 at the VEPP-2M[14] collider in the energy range $\sqrt{s}$ from 360 to 1400 MeV. The detector contains several subsystems. The tracking system includes two cylindrical drift chambers. The three-layer spherical electromagnetic calorimeter is based on NaI(Tl) crystals. The muon/veto system consists of plastic scintillation counters and two layers of streamer tubes. The calorimeter energy and angular resolution depend on the photon energy as $\sigma_E/E(\%) = 4.2\%/\sqrt[4]{E(\text{GeV})}$ and $\sigma_{\phi,\theta} = 0.82^\circ/\sqrt{E(\text{GeV})} \oplus 0.63^\circ$. The tracking system angular resolution is about 0.5° and 2° for azimuthal and polar angles respectively. The energy loss resolution dE/dx in the drift chamber is about 30% – good enough to provide charged kaon identification in the ϕ-meson production region.

In 1998 SND had collected data in the energy region from 984 to 1060 MeV[7] with integrated luminosity about 8.5 pb^{-1}. For studies of the dipion mass spectra in the process $e^+e^- \to \pi^+\pi^-\pi^0$ the data sample collected in the energy region $\sqrt{s} = 1016$ – 1022 MeV was used. The total integrated luminosity accumulated in this region is about 4.3 pb^{-1}.

B. Selection of $e^+e^- \to \pi^+\pi^-\pi^0$ events

The data analysis and selection criteria used in this work are similar to those described in Ref.[7]. During the experimental runs, the first-level trigger[13] selects events with energy deposition in the calorimeter more then 200 MeV and containing two or more charged particles. During processing of the experimental data the event reconstruction is performed[13,7]. For further analysis events containing two or more photons and two charged particles with $|z| < 10$ cm and $r < 1$ cm were selected. Here z is the coordinate of the charged particle production point along the beam axis (the longitudinal size of the interaction region is $\sigma_z \sim 2.5$ cm); r is the distance between the charged particle track and the beam axis in the $r - \phi$ plane. Extra photons in $e^+e^- \to \pi^+\pi^-\pi^0$ events can appear because of the beam background overlap or nuclear interactions of the charged pions in the calorimeter. Under these selection conditions, the background sources are $e^+e^- \to K^+K^-$, K_SK_L, $\eta\gamma$, $\omega\pi^0$, $e^+e^-\gamma\gamma$ processes and the beam background.

To suppress the beam background, the following cuts on the angle between the two charged particles tracks ψ and energy deposition of the neutral particles E_{neu} were applied: $\psi > 40^\circ$, $E_{neu} > 0.1 \cdot\sqrt{s}$.

To reject the background from the $e^+e^- \to K^+K^-$ process the following cuts were imposed: $(dE/dx) < 5 \cdot (dE/dx)_{min}$ for each charged particle, $(dE/dx) < 3 \cdot (dE/dx)_{min}$ at least for one of them, and $\Delta\phi < 10^\circ$. Here $|\Delta\phi|$ is an acollinearity angle in the azimuthal plane and $(dE/dx)_{min}$ is an average energy loss of a minimum ionizing particle. To suppress the $e^+e^- \to e^+e^-\gamma\gamma$ events the energy deposition of the charged particles E_{cha} was required to be small enough: $E_{cha} < 0.5 \cdot\sqrt{s}$.

The selected events were reconstructed under assumption that all registered particles have the common vertex in the e^+e^- interaction region. The average position of the beams interaction point and its *rms* spread were measured by using $e^+e^- \to e^+e^-$ events during data collection. Then a kinematic fit was performed under the following constraints: the charged particles are considered to be pions, the system has zero total momentum, the total energy is $\sqrt{s}$, and the photons originate from the $\pi^0 \to \gamma\gamma$ decays. The value of the likelihood function $\chi^2_{3\pi}$ is calculated during the fit. In events with more than two photons, extra photons are considered as spurious ones and rejected. To do this, all possible subsets of two photons were inspected and the one, corresponding to the maximum likelihood was selected. The two-photon invariant mass and $\chi^2_{3\pi}$ distributions are shown in Fig.2 and Fig.3. After the kinematic fit the following additional cuts were applied: $36^\circ < \theta_\gamma < 144^\circ$, $N_\gamma = 2$, and $\chi^2_{3\pi} < 20$. Here θ_γ is polar angle of one of the photons selected by the reconstruction program as originated from the π^0-decay, N_γ is the number of detected photons. Under these criteria about 0.5×10^6 events were selected. In Fig.4 and Fig.5 the angular distributions of pions for the selected events are shown. While Fig.6 and Fig.7 demonstrates the photon energy distributions for the same events.

The difference between described selection criteria and those used in Ref.[7] is that the cuts on the pion and photon angles were relaxed here. This leads to the increase of the selected events number by a factor of about 1.5. The ϕ meson parameters obtained under this new selection criteria agree with results reported in the previous work. For example, the $e^+e^- \to \pi^+\pi^-\pi^0$ cross section changed by about 0.5%, what is negligible in comparison with the 5% systematic error declared in Ref.[7].

The number of background events was estimated by using simulation in the following way:

$$N_{bkg}(s) = \sum_i \sigma_{Ri}(s)\epsilon_i(s)IL(s), \qquad (1)$$

where i is a process number, $\sigma_{Ri}(s)$ is the cross section of the background process taking into account the radiative corrections, $IL(s)$ is the integrated luminosity, $\epsilon_i(s)$ is the detection probability for the background process. The accuracy of the background events number determination is estimated to be about 15 – 20 %. The numbers of $e^+e^- \to \pi^+\pi^-\pi^0$ events (after background subtraction) and background event numbers are shown in Table I. The $e^+e^- \to K_SK_L$ events are the main background source and their contribution is $\sim 1\%$ of all selected events.

C. Construction of the $\pi^+\pi^-$ and $\pi^\pm\pi^0$ mass spectra

For the selected events the $\pi^+\pi^-$ and $\pi^\pm\pi^0$ mass spectra were formed and arranged in histograms with dipion mass range from 280 to 880 MeV and bin width of 20 MeV. All experimental energy points were used to produce a single invariant mass distribution. In case of the $\pi^\pm\pi^0$ distribution the charged pion was selected at random from the two possibilities. The invariant mass values were calculated after the kinematic reconstruction.

The expected background was subtracted bin by bin while forming the desired histograms. Simulated distributions were used for subtraction of the $e^+e^- \to K^+K^-$, $\eta\gamma$, $\omega\pi^0$ and $e^+e^-\gamma\gamma$ backgrounds. The $e^+e^- \to K_SK_L$ main background was studied using experimental events.

As a rule, the background from the $e^+e^- \to K_SK_L$ originates when $K_S \to \pi^+\pi^-$ decay inside the collider vacuum chamber is accompanied by "photons" in calorimeter produced due to K_L meson nuclear interactions or its decay in flight inside the calorimeter. To select K_SK_L events for related background studies the following additional cuts were applied $r > 0.2$ cm for both charged particles and $\psi > 130^\circ$. Note that K_S decay length is about 0.5 cm for our energies and the angle ψ between the pions from the K_S decay is about 150°.

The experimental and simulated "$\pi^\pm\pi^0$" distributions are consistent to each other (Fig.8), so the simulated distribution was used for the K_SK_L background subtraction in the $\pi^\pm\pi^0$ invariant mass spectrum. The agreement is not so good for the "$\pi^+\pi^-$" mass spectrum: the simulated histogram is shifted from the experimental one by about 3% in the peak region (Fig.9). This disagreement is caused due to inaccuracies in simulation of the K_L nuclear interactions. The experimental distribution (Fig.9) was used for K_SK_L background subtraction for events in which both charged particles had $r > 0.2$ cm. Unfortunately, this procedure is not justified if at least one charged particle in the event has $r < 0.2$ cm. Indeed, "$\pi^+\pi^-$" mass distribution for the K_SK_L background depends crucially on the shape of the angle ψ distribution, which in its turn depends on the value of r, because during event reconstruction it was assumed that all charged particle tracks have a common vertex in the beams interaction region. For the $K_S \to \pi^+\pi^-$ vertex this assumption is not true. Therefore, "$\pi^+\pi^-$" distribution obtained for K_SK_L background under condition $r > 0.2$ cm cannot be used for subtraction of all K_SK_L background. Instead for events with $r < 0.2$ cm for one of the charged particles the simulated distribution, corrected for the above mentioned 3% discrepancy, was used for K_SK_L background subtraction. The dipion invariant mass spectra and background contributions obtained in such a way are shown in Fig.10, 11.

III. THEORETICAL FRAMEWORK

In the VDM framework the cross section of the $e^+e^- \to \pi^+\pi^-\pi^0$ process is

$$\frac{d\sigma}{dm_0 dm_+} = \frac{4\pi\alpha}{s^{3/2}}\left|A_{\rho\pi}(s)\right|^2 \frac{|\vec{p}_+ \times \vec{p}_-|^2}{12\pi^2\sqrt{s}} m_0 m_+ \cdot |F|^2, \tag{2}$$

where $\vec{p}_+$ and $\vec{p}_-$ are the π^+ and π^- momenta, m_0 and m_+ are $\pi^+\pi^-$ and $\pi^+\pi^0$ invariant masses. Formfactor F of the $\gamma^\star \to \pi^+\pi^-\pi^0$ transition has the form

$$|F|^2 = \left| \frac{g_{\rho^0\pi\pi}}{D_\rho(m_0)Z(m_0)} + \frac{g_{\rho^+\pi\pi}}{D_{\rho^+}(m_+)Z(m_+)} + \frac{g_{\rho^-\pi\pi}}{D_{\rho^-}(m_-)Z(m_-)} + \frac{A_{\omega\pi}(s)}{A_{\rho\pi}(s)} \frac{\Pi_{\rho\omega} g_{\rho^0\pi\pi}}{D_\rho(m_0)D_\omega(m_0)} + a_{3\pi} \right|^2 \tag{3}$$

Here

$$D_\rho(m_0) = m_{\rho^0}^2 - m_0^2 - i m_0 \Gamma_{\rho^0}(m_0), \quad D_{\rho^\pm}(m_\pm) = m_{\rho^\pm}^2 - m_\pm^2 - i m_\pm \Gamma_{\rho^\pm}(m_\pm)$$

$$\Gamma_{\rho^0}(m_0) = \left(\frac{m_{\rho^0}}{m_0}\right)^2 \Gamma_{\rho^0} \left(\frac{q_0(m_0)}{q_0(m_{\rho^0})}\right)^3, \quad \Gamma_{\rho^\pm}(m_\pm) = \left(\frac{m_{\rho^\pm}}{m_\pm}\right)^2 \Gamma_{\rho^\pm} \left(\frac{q_\pm(m_\pm)}{q_\pm(m_{\rho^\pm})}\right)^3,$$

$$q_0(m) = \frac{1}{2}(m^2 - 4m_\pi^2)^{1/2}, q_\pm(m) = \frac{1}{2m}((m^2-(m_{\pi^0}+m_\pi)^2)(m^2-(m_{\pi^0}-m_\pi)^2)^{1/2},$$

$$m_- = \sqrt{s + m_{\pi^0}^2 + 2m_\pi^2 - m_0^2 - m_+^2},$$

where m_- is $\pi^-\pi^0$ invariant mass, m_{π^0} and m_π are the neutral and charged pion masses. The $\rho^0 \to \pi^+\pi^-$ and $\rho^\pm \to \pi^\pm\pi^0$ transition coupling constants could be determined in the following way:

$$g^2_{\rho^0\pi\pi} = \frac{6\pi m^2_{\rho^0}\Gamma_{\rho^0}}{q_0(m_{\rho^0})^3}, \quad g^2_{\rho^\pm\pi\pi} = \frac{6\pi m^2_{\rho^\pm}\Gamma_{\rho^\pm}}{q_\pm(m_{\rho^\pm})^3}$$

If these constants are equal, then the ρ^0 and $\rho^\pm$ meson widths are related as follows:

$$\Gamma_{\rho^\pm} = \Gamma_{\rho^0}\frac{m^2_{\rho^0}}{m^2_{\rho^\pm}}\frac{q_\pm(m_{\rho^\pm})^3}{q_0(m_{\rho^0})^3} \tag{4}$$

Factor $Z(m) = 1 - is_1\Phi(m,s)$ takes into account the interaction of the ρ and π mesons in the final state[10]. $\Phi(m,s)$ as a function of the pion pair invariant mass m is shown in Fig.12 for the e^+e^- center-of-mass energy $\sqrt{s} = m_\phi$. The free parameter in our fit s_1 was introduced to account for possible deviations from the Ref.[10] prediction $s_1 = 1$. The fourth item in (3) takes into account the $\rho - \omega$ mixing[15]. Polarization operator of these mixing $\Pi_{\rho\omega}$ satisfies $\mathrm{Im}(\Pi_{\rho\omega}) \ll \mathrm{Re}(\Pi_{\rho\omega})$, where $\mathrm{Re}(\Pi_{\rho\omega}) = 2m_\omega\delta$ with $\delta = 2.3$ MeV[10,16]. So we have assumed $\mathrm{Im}(\Pi_{\rho\omega}) = 0$ in subsequent analysis. Amplitudes of the $\gamma^\star \to \rho\pi$ and $\gamma^\star \to \omega\pi^0$ transitions have the form

$$A_{\rho\pi}(s) = \sum_{V=\omega,\phi,\omega',\omega''}\frac{g_{\gamma V}g_{V\rho\pi}}{D_V(s)}, \quad A_{\omega\pi}(s) = \sum_{V=\rho,\rho',\rho''}\frac{g_{\gamma V}g_{V\omega\pi^0}}{D_V(s)}, \tag{5}$$

Using SND measurements of the $e^+e^- \to \pi^+\pi^-\pi^0$ and $e^+e^- \to \pi^0\pi^0\gamma$ cross sections[7,17], we can express the ratio of these amplitudes in the ϕ-meson region as

$$A_{\omega\pi}(s)/A_{\rho\pi}(s) = K_{\omega\pi/\rho\pi}e^{i\phi_{\omega\pi/\rho\pi}}, K_{\omega\pi/\rho\pi} \simeq 0.3, \phi_{\omega\pi/\rho\pi} \simeq -110^\circ, \sqrt{s} = m_\phi.$$

The amplitude $a_{3\pi}$ takes into account possible additional intermediate states in the $\gamma^\star \to \pi^+\pi^-\pi^0$ transition. For example, $\gamma^\star \to \rho'(\rho'')\pi \to \pi^+\pi^-\pi^0$ transition will lead to the contribution

$$a_{3\pi} = \frac{A_{\rho'\pi}(s)}{A_{\rho\pi}(s)}\left(\frac{g_{\rho'\pi\pi}}{D_{\rho'}(m_0)} + \frac{g_{\rho'\pi\pi}}{D_{\rho'}(m_+)} + \frac{g_{\rho'\pi\pi}}{D_{\rho'}(m_-)}\right), \tag{6}$$

where

$$A_{\rho'\pi}(s) = \sum_{V=\omega,\phi,\omega'}\frac{g_{\gamma V}g_{V\rho'\pi}}{D_V(s)}. \tag{7}$$

The ratio $A_{\rho'\pi}/A_{\rho\pi}$ is expected to be real for energies $\sqrt{s} \simeq m_\phi$[18] where

$$\frac{A_{\rho'\pi}}{A_{\rho\pi}} \simeq \frac{g_{\phi\rho'\pi}}{g_{\phi\rho\pi}}.$$

So the imaginary part of (6) is negligible due to the large ρ' mass ($m_{\rho'} \sim 1400$ MeV). Therefore the $a_{3\pi}$ amplitude was assumed to be real in our analysis.

IV. APPROXIMATION OF THE $\pi\pi$ MASS SPECTRA

A. Theoretical distributions

The experimental dipion mass spectra (Tables II and III) were fitted with theoretical distributions. Using the $e^+e^- \to \pi^+\pi^-\pi^0$ cross section (2) the theoretical spectra were calculated in the following way:

$$S_j^{(0)}(s) = \frac{1}{C_S(s)} \cdot \int\limits_{m_j-\Delta}^{m_j+\Delta} m_0 dm_0 \int\limits_{m_+^{min}(m_0)}^{m_+^{max}(m_0)} m_+ dm_+ |\vec{p}_+ \times \vec{p}_-|^2 \cdot |F|^2, \tag{8}$$

$$S_j^{(\pm)}(s) = \frac{1}{C_S(s)} \cdot \int\limits_{m_j-\Delta}^{m_j+\Delta} m_\pm dm_\pm \int\limits_{m_0^{min}(m_+)}^{m_0^{max}(m_+)} m_0 dm_0 |\vec{p}_+ \times \vec{p}_-|^2 \cdot |F|^2, \tag{9}$$

where j is the bin number, $\Delta = 10$ MeV - half of the bin width, m_j - the central value of the invariant mass in the jth bin, $C_S(s)$ - normalizing coefficient. These spectra were corrected taking into account the detection efficiency ϵ_j (Fig.13 and 14) for the jth bin and a probability a_{ij} for the event belonging to the jth bin to migrate to the ith bin due to finite detector resolution

$$G_i^{(0)}(s) = \left(\sum_j a_{ij}^{(0)} S_j^{(0)}(s) \epsilon_j^{(0)} \right) \cdot (1 + \delta_i^{(0)}(s)) \cdot \beta_i^{(0)} \tag{10}$$

$$G_i^{(\pm)}(s) = \left(\sum_j a_{ij}^{(\pm)} S_j^{(\pm)}(s) \epsilon_j^{(\pm)} \right) \cdot (1 + \delta_i^{(\pm)}(s)) \cdot \beta_i^{(\pm)} \tag{11}$$

Here $\delta_i(s)$ is a radiative correction, $\beta_i^{(0)}$ and $\beta_i^{(\pm)}$ are corrections due to inaccuracies in simulation of the nuclear interactions of the charged pions. The values of a_{ij}, ϵ_j and $\delta_i(s)$ were obtained from simulation.

These distributions were formed for all energy points $\sqrt{s}$ (Table I) and then summed as follows:

$$P_i^{(0)} = \sum_s w(s) \cdot \frac{G_i^{(0)}(s)}{C_G(s)}, \quad P_i^{(\pm)} = \sum_s w(s) \cdot \frac{G_i^{(\pm)}(s)}{C_G(s)} \tag{12}$$

Here $C_G(s) = \sum_i G_i(s)$ is a normalization factor, $w(s) = N(s)/N$ is the weight factor, $N(s)$ and N being the numbers of the $e^+e^- \to \pi^+\pi^-\pi^0$ events in each energy point and the total events number respectively (Table I).

B. Detection efficiency

To obtain the a_{ij}, ϵ_j and $\delta_i(s)$, the Monte-Carlo sample of about 1.4×10^6 $e^+e^- \to \rho\pi \to \pi^+\pi^-\pi^0$ events were processed in the same way as experimental data. The statistical errors of a_{ij} coefficients were included in the error of P_i (Tables.II and III). The average detection efficiency obtained by simulation is about 0.37 and varies from 0.05 to 0.4 depending on dipion mass value (Fig. 13 and 14).

Inaccuracies in the $\chi^2_{3\pi}$ and dE/dx simulations lead to an error in average detection efficiency[7], but do not modify its dependence on the $\pi\pi$ invariant mass, except the regions of $m_{\pi\pi} < 315$ MeV and $m_{\pi\pi} > 845$ MeV. The cut $N_\gamma = 2$ is also a source of some error in the detection efficiency determination, due to inaccuracies in the extra photons simulation. As was mentioned above, extra photons can appear because of the beam background overlap or charged pion nuclear interactions. In fact, if the extra photons originate from the beam background overlap, $N_\gamma = 2$ criteria does not modify the detection efficiency dependence on a dipion mass, because the probability of beam background overlap does not depend on dipion mass. On the contrary, the probability of extra photons appearance because of nuclear interactions of the charged pions does depend on pion energy. Therefore any inaccuracy in simulation of these nuclear interactions will transform in inaccuracies in the simulation of extra photons and can lead to the detection efficiency error which will depend on the dipion mass. To correct this error we used the correction factor obtained in the following way:

$$\beta_i^{(0)} = \frac{n_i^{(0)}/N_i^{(0)}}{k_i^{(0)}/K_i^{(0)}}, \quad \beta_i^{(\pm)} = \frac{n_i^{(\pm)}/N_i^{(\pm)}}{k_i^{(\pm)}/K_i^{(\pm)}}, \tag{13}$$

where K_i and N_i are the event numbers in the ith bin of experimental and simulated mass spectra respectively under condition $N_\gamma \geq 2$. k_i and n_i are the event numbers when the cut $N_\gamma = 2$ was imposed. The dependence of these correction factors on the dipion mass (Fig.15) can be approximated by linear functions:

$$\beta_i^{(0)} = C^{(0)} \cdot (1 + a_0 \cdot m_i), \quad \beta_i^{(\pm)} = C^{(\pm)} \cdot (1 + a_\pm \cdot m_i)$$

with slopes $a_0 = -0.13 \cdot 10^{-3}$ and $a_\pm = 0.083 \cdot 10^{-3}$ for $\pi^+\pi^-$ and $\pi^\pm\pi^0$ pairs respectively. As was mentioned above, the detection efficiency in the regions $m_{\pi\pi} <$ 315 MeV and $m_{\pi\pi} > 845$ MeV have a large error. Uncertenity of P_i in these regions was increased by addition of the 100% spread.

C. Fitting of the experimental distributions

The $\pi^+\pi^-$ and $\pi^\pm\pi^0$ mass spectra were fitted together. The function to be minimized was $\chi^2 = \chi^2_0 + \chi^2_\pm$, where

$$\chi^2_0 = \sum_i \left(\frac{H_i^{(0)} - P_i^{(0)}}{\sigma_i^{(0)}} \right)^2, \quad \chi^2_\pm = \sum_i \left(\frac{H_i^{(\pm)} - P_i^{(\pm)}}{\sigma_i^{(\pm)}} \right)^2. \tag{14}$$

Here $H^{(0)}$ and $H^{(\pm)}$ are the normalized $\pi^+\pi^-$ and $\pi^\pm\pi^0$ mass distributions (histograms); $\sigma_i^{(0)} = \Delta H_i^{(0)} \oplus \Delta P_i^{(0)}$ and $\sigma_i^{(\pm)} = \Delta H_i^{(\pm)} \oplus \Delta P_i^{(\pm)}$ include the uncertainties ΔH_i and ΔP_i of the experimental and theoretical distributions.

The fitting was performed with m_{ρ^0}, $m_{\rho^\pm} - m_{\rho^0}$, Γ_{ρ^0}, $\Gamma_{\rho^\pm}$ as free parameters under the following assumptions:

1. $a_{3\pi} = 0$, $K_{\omega\pi/\rho\pi} = 0$, $s_1 = 0$;

2. $a_{3\pi}$ was free parameter, $K_{\omega\pi/\rho\pi} = 0$, $s_1 = 0$;

3. $a_{3\pi} = 0$, $K_{\omega\pi/\rho\pi}$ and $\phi_{\omega\pi/\rho\pi}$ were free parameters, $s_1 = 0$;

4. $a_{3\pi} = 0$, $K_{\omega\pi/\rho\pi} = 0$, s_1 was free parameter.

The χ^2 value for all variants approximately equals to 73 for $54-52$ degrees of freedom, besides $\chi^2_0 \simeq 44$, $\chi^2_\pm \simeq 29$. The difference $H_i - P_i$ between the experimental and theoretic spectra are shown in Fig.16 and 17. The difference for the $\pi^+\pi^-$ distribution has a systematic spread of about 1%. This spread was added to uncertainty of the theoretical $P_i^{(0)}$ distribution and the fit was redone (Table.IV). For all variants of fitting the values of ρ meson widths Γ_{ρ^0} and $\Gamma_{\rho^\pm}$ are consistent with relation (4), and fits were performed again under assumption that $g_{\rho^0\pi\pi} = g_{\rho^\pm\pi\pi}$ (Table.V) (Γ_{ρ^0} was free parameter and $\Gamma_{\rho^\pm}$ was calculated using expression (4)). The ρ^0 and $\rho^\pm$ mass difference is consistent with zero, and the fits were redone again under assumption $m_{\rho^\pm} = m_{\rho^0}$ (Table VI). The experimental spectra fitted with theoretical distributions (variant 3 in Table VI) are shown in Fig.18 and 19.

The parameters determined by fit are subject of various systematic errors originated from model dependence, from inaccuracy in background subtraction and in detection efficiency determination. To estimate errors due to uncertainty in background subtraction the experimental distributions were approximated with the sum of three histograms corresponding to the theoretical spectrum for the effect, K_SK_L background and expected summary background from sources other then K_SK_L. The background events fractions were taken as free parameters of the fit. The values of these fractions obtained from the fit differs by less than 20% from those estimated using equation (1).

To study systematics related to inaccuracy in the extra photons simulation the corresponding correction factors were approximated by assuming the higher order polynomial, instead of linear function, to fit the dependence of these factors on the dipion mass shown in Fig.15. We also had tried the fit with linear approximation for the correction factors but with a_0 and $a_\pm$ as free parameters of the fit. The results of the fit $a_0 = (-0.13 \pm 0.02) \cdot 10^{-3}$ and $a_\pm = (0.12 \pm 0.2) \cdot 10^{-3}$ are consistent with those described above.

The model dependence was estimated by using results of the fits performed under different assumptions (Tables IV, V, VI).

V. DISCUSSION

The SND results in comparison with other experimental data are shown in Table VII.

The fit results revealed that the experimental data can be described by using only $\rho\pi$ intermediate state. The value of additional, other than $\rho\pi$, contribution $a_{3\pi}$ is consistent with zero (variant 2, in Table VI):

$$a_{3\pi} = (0.01 \pm 0.23 \pm 0.25) \times 10^{-5} \ \ \mathrm{MeV}^{-2},$$

Here the systematic error is related to uncertainties in background subtraction and detection efficiency determination. This result agrees with $a_{3\pi} = (0.08 \pm 0.45 \pm 0.37) \times 10^{-5}$ MeV^{-2} reported in Ref.[6]. Using the $a_{3\pi}$ value and results of the $e^+e^- \to \pi^+\pi^-\pi^0$ cross section study[7] the upper limit on the branching ratio of $\phi \to \pi^+\pi^-\pi^0$ decay without the $\rho\pi$ intermediate state can be obtained:

$$B(\phi \to \pi^+\pi^-\pi^0) < 6 \cdot 10^{-4} \ \ (90\% \ \mathrm{CL})$$

This upper limit implies

$$0.91 < \frac{\sigma_{3\pi}}{\sigma_{\rho\pi}} < 1.09 \ \ (90\% \ \mathrm{CL})$$

Here $\sigma_{3\pi}$ is the total $e^+e^- \to \pi^+\pi^-\pi^0$ cross section, $\sigma_{\rho\pi}$ is $e^+e^- \to \rho\pi \to \pi^+\pi^-\pi^0$ cross section. The upper and lower limits above correspond to the constructive and destructive interference between $a_{3\pi}$ and $\rho\pi$ related amplitudes. It may happen that $e^+e^- \to \phi \to \rho'\pi$ amplitude is suppressed compared to $e^+e^- \to \omega(\omega') \to \rho'\pi$ amplitude. In this case one expects $\mathrm{Im}(a_{3\pi}) > \mathrm{Re}(a_{3\pi})$. So we had performed also the fit with $\mathrm{Im}(a_{3\pi})$ as free parameter and supposing $\mathrm{Re}(a_{3\pi}) = 0$. The result of this fit also is consistent with zero:

$$a_{3\pi} = i \cdot (-0.12 \pm 0.13 \pm 0.25)$$

The fit with model taking into account $\rho-\omega$ mixing (variant 3 in Table VI) gave the results

$$K_{\omega\pi/\rho\pi} = 0.20 \pm 0.10 \pm 0.05 \quad \phi_{\omega\pi/\rho\pi} = -125^\circ \pm 28^\circ.$$

The systematic error is related to uncertenity in background subtraction. The values obtained are consistent to the above given estimation $K_{\omega\pi/\rho\pi} \simeq 0.3$, $\phi_{\omega\pi/\rho\pi} \simeq -110^\circ$. The measured value of $K_{\omega\pi/\rho\pi}$ deviates from zero by about two standard deviations.

Parameter s_1 is related to the final state interaction of the ρ and π mesons and was measured to be (variant 5 in Table VI):

$$s_1 = 0.3 \pm 0.3 \pm 0.3$$

The main cause of the systematic error is again the background subtraction uncertenity. The result is consistent with zero, but also does not contradict to the prediction of Ref.[10] ($s_1 = 1$ with about 10-20% accuracy).

The measured neutral and charged ρ-mesons masses and their difference are (variant 1 in Table V):

$$m_{\rho^0} = 775.8 \pm 0.9 \pm 2.0 \ \ \mathrm{MeV},\ m_{\rho^\pm} = 774.5 \pm 0.7 \pm 1.5 \ \ \mathrm{MeV},$$

$$m_{\rho^\pm} - m_{\rho^0} = -1.3 \pm 1.1 \pm 2.0 \ \ \mathrm{MeV}.$$

The systematic error of $m_{\rho^\pm}$ is related to model dependence and uncertainties in detection efficiency determination. Background subtraction inaccuracy also contributes in the systematic errors of m_{ρ^0} and $m_{\rho^\pm} - m_{\rho^0}$. The results obtained are consistent with $m_{\rho^\pm} = m_{\rho^0}$ as well as with the world average for the mass difference -0.4 ± 0.8 MeV[12]. The measured mass difference is also not in conflict with the prediction $m_{\rho^\pm} - m_{\rho^0} = -4.2 \pm 1.2$ MeV[11]. If $m_{\rho^\pm} = m_{\rho^0}$ is assumed in the fit, the ρ-meson mass turns out to be (variant 1 from Table.VI):

$$m_\rho = 775.0 \pm 0.6 \pm 1.1 \ \ \mathrm{MeV}$$

This value is consistent with the results of the e^+e^- annihilation and τ decay experiments (Table VII). Note that world average for these experiments is $m_\rho = 776 \pm 0.9$ MeV. But the PDG value[12] 769.3 ± 0.8 MeV, which takes into account all experiments in which the ρ-meson mass was measured, contradicts to the reported SND result.

Our results for the neutral and charged ρ-meson widths are (variant 1 Table IV):

$$\Gamma_{\rho^0} = 151.1 \pm 2.6 \pm 3.0 \ \ \mathrm{MeV},\ \Gamma_{\rho^\pm} = 149.9 \pm 2.3 \pm 2.0 \ \ \mathrm{MeV}$$

The systematic error includes model dependence, uncertainty in background subtraction and in detection efficiency determination. Under assumption $g_{\rho^0\pi\pi} = g_{\rho^\pm\pi\pi}$ (variant 1 Table VI) the ρ-meson widths were found to be

$$\Gamma_{\rho^0} = 149.8 \pm 2.2 \pm 2.0 \ \ \mathrm{MeV},\ \Gamma_{\rho^\pm} = 150.9 \pm 2.2 \pm 2.0 \ \ \mathrm{MeV}$$

These results are consistent with other experimental results (Table VII) as well as with the PDG world average 150.2 ± 0.8 MeV[12].

VI. CONCLUSIONS

In the SND experiment at VEPP-2M collider in Novosibirsk the dipion mass spectra were studied in the $e^+e^- \to \pi^+\pi^-\pi^0$ process at $\sqrt{s} = m_\phi$. The study is based on the data sample with about 0.5×10^6 experimental events. Spectra were analyzed within the VDM framework taking into account $e^+e^- \to \rho\pi$ transition, $\rho - \omega$ mixing, final state interaction of the ρ and π mesons, possible transition $e^+e^- \to \pi^+\pi^-\pi^0$ through intermediate states different from $\rho\pi$ (for example, via $\rho'\pi$). Within the limits of our accuracy, the experimental data can be described with the $e^+e^- \to \rho\pi \to \pi^+\pi^-\pi^0$ transition only. The upper limit on the $\phi \to 3\pi$ decay through intermediate states besides $\rho\pi$ is $B(\phi \to \pi^+\pi^-\pi^0) < 6 \cdot 10^{-4}$. In the $\pi^+\pi^-$ invariant mass spectrum the $\rho - \omega$ interference was observed at two standard deviations level. The measured mass and width values for the neutral and charged ρ-mesons are $m_{\rho^0} = 775.8 \pm 0.9 \pm 2.0$ MeV, $\Gamma_{\rho^0} = 151.1 \pm 2.6 \pm 3.0$ MeV, $m_{\rho^\pm} = 774.5 \pm 0.7 \pm 1.5$ MeV, $\Gamma_{\rho^\pm} = 149.9 \pm 2.3 \pm 2.0$ MeV. The difference between masses of the neutral and charged ρ-mesons was found to be $m_{\rho^\pm} - m_{\rho^0} = -1.3 \pm 1.1 \pm 2.0$ MeV. Under assumption $m_{\rho^\pm} = m_{\rho^0}$ the following ρ-meson mass value was obtained $m_\rho = 775.0 \pm 0.6 \pm 1.1$ MeV. Assuming the coupling constants equality $g_{\rho^0\pi\pi} = g_{\rho^\pm\pi\pi}$, the neutral and charged ρ-meson widths turn out to be $\Gamma_{\rho^0} = 149.8 \pm 2.2 \pm 2.0$ MeV and $\Gamma_{\rho^\pm} = 150.9 \pm 2.2 \pm 2.0$ MeV.

ACKNOWLEDGMENTS

The authors are grateful to N.N.Achasov and A.A.Kozhevnikov for useful discussions.

---

[1] G. Parrour et al., Phys. Lett. **B 63**, 357 (1976).

[2] A.D. Bukin et al., Yad. Fiz. **27**, 976 (1978) [Sov. J. of Nucl. Phys. **27**, 516 (1978)].

[3] A. Cordier et al., Phys. Lett. **B 364**, 13 (1980)

[4] S.I. Dolinsky et al., Phys. Rep. **202**, 99 (1991)

[5] R.R. Akhmetshin et al., Phys. Lett. **B 364**, 199 (1995)

[6] B.R. Akhmetshin et al., Phys. Lett. **B 434**, 426 (1998)

[7] M.N. Achasov et al., Phys. Rev. **D 63**, 072002 (2001)

[8] G. Parrour et al., Phys. Lett. **B 63**, 362 (1976)

[9] M.N. Achasov et al., Preprint Budker INP 98-65 Novosibirsk, 1998

[10] N.N. Achasov and A.A. Kozhevnikov, Phys. Rev. **D 49**, 5773 (1994)
Yad. Fiz. 56, 191 (1993) [Phys. Atom. Nucl. 56, 1261 (1993)]
Int. J. Mod. Phys. **A 9**, 527 (1994)

[11] M.N. Achasov and N.N. Achasov, Pis'ma Zh. Eksp. Teor. Fiz. 69, 8 (1999) [JETP Lett. 69, 7 (1999)].

[12] Particle Data Group, D.E. Groom, et al., Eur.Phys.J. **C 15**, 1 (2000)

[13] M.N. Achasov et al., Nucl. Instr. and Meth. **A 449**, 125 (2000)

[14] A.N. Skrinsky, in Proc. of Workshop on physics and detectors for DAΦNE, Frascati, Italy, April 4-7, 1995, p.3

[15] N.N. Achasov, A.A. Kozhevnikov, and G.N. Shestakov, Phys. Lett. **50B**, 448 (1974) .
N.N. Achasov, N.M. Budnev, A.A. Kozhevnikov, and G.N. Shestakov, Yad. Fiz. 23, 610 (1976) [Sov. J. Nucl. Phys. 23, 320 (1976)];
N.N. Achasov and G.N. Shestakov, Fiz. Elem. Chastits. At. Yadra 9, 48 (1978)

[16] N.N. Achasov and A.A. Kozhevnikov, Yad. Fiz. 55, 809 (1992) [Sov. J. Nucl. Phys. 55, 449 (1992)];
Int. J. Mod. Phys. **A 7**, 4825 (1992).
[17] M.N.Achasov et al., Phys. Lett. **B 486**, 29 (2000)
[18] N.N. Achasov and A.A.Kozhevnikov, Yad. Fiz. 55, 3086 (1992) [Sov. J. Nucl. Phys. 55, 1726 (1992)];
Phys. Rev. **D 61**, 054005 (2000);
Yad. Fiz. 63, 2029 (2000) [Phys. At. Nucl. 63, 1936 (2000)]
[19] R.R.Akhmetshin et al., Preprint Budker INP 99-10 Novosibirsk, 1999
[20] R.Barate et al., Z.Phys. **C 76**, 15 (1997)
[21] S.Anderson et al., Phys. Rev, **D 61**, 112002 (2000)
[22] A. Abele et al., Phys. Lett. **B 469**, 270 (1999)

$\sqrt{s}$ (MeV)	$N_{3\pi}$	N_{bkg}	$N_{K_SK_L}$	$N_{K^+K^-}$	$N_{\eta\gamma}$	$N_{\omega\pi}$	$N_{2e2\gamma}$
~ 1017	45913	410	331	3	42	15	19
~ 1018	101651	1067	901	8	104	24	29
~ 1019	137432	1696	1465	13	161	26	31
~ 1020	139319	1871	1674	12	147	27	31
~ 1021	68074	1024	903	7	78	17	20
	492389	6088	5274	43	532	109	130

TABLE I. Event numbers for the effect and estimated background at various energies. $N_{3\pi}$ - number of selected $e^+e^- \to \pi^+\pi^-\pi^0$ events after background subtraction. N_{bkg} - the total estimated background. Contributions of separate background sources are also shown. The last line contains the total events numbers for all energy points.

i	m_i (MeV)	$b^{(0)}_{i,i-4}$	$b^{(0)}_{i,i-3}$	$b^{(0)}_{i,i-2}$	$b^{(0)}_{i,i-1}$	$b^{(0)}_{i,i}$	$b^{(0)}_{i,i+1}$	$b^{(0)}_{i,i+2}$	$b^{(0)}_{i,i+3}$	$\delta P^{(0)}_i$	$H^{(0)}_i \cdot 10^4$
1	290	–	–	–	–	0.001	0.002	–	–	1.055	0.10 ± 0.04
2	310	–	–	–	–	0.015	0.009	0.001	–	1.004	3.0 ± 0.3
3	330	–	–	–	0.009	0.210	0.035	0.001	–	0.018	49.6 ± 1.1
4	350	–	0.001	0.002	0.026	0.295	0.045	0.002	0.001	0.015	103.6 ± 1.5
5	370	–	0.001	0.001	0.028	0.302	0.051	0.003	0.001	0.014	154.0 ± 1.9
6	390	0.001	0.001	0.003	0.034	0.317	0.058	0.003	0.001	0.013	212.5 ± 2.3
7	410	0.001	0.001	0.002	0.036	0.316	0.061	0.003	0.001	0.012	267.9 ± 2.5
8	430	–	–	0.001	0.040	0.313	0.065	0.004	0.001	0.012	322.9 ± 2.8
9	450	–	–	0.002	0.047	0.304	0.070	0.004	0.001	0.012	378.2 ± 3.0
10	470	–	–	0.002	0.050	0.292	0.071	0.005	0.001	0.012	434.7 ± 3.2
11	490	–	0.001	0.003	0.058	0.291	0.075	0.005	0.001	0.011	485.9 ± 3.4
12	510	–	0.001	0.003	0.061	0.273	0.073	0.006	0.001	0.011	539.0 ± 3.6
13	530	–	–	0.004	0.065	0.271	0.076	0.006	0.001	0.011	578.3 ± 3.8
14	550	–	0.001	0.005	0.067	0.258	0.073	0.006	0.001	0.011	614.6 ± 3.9
15	570	–	0.001	0.005	0.070	0.249	0.073	0.006	0.001	0.011	645.6 ± 4.0
16	590	–	0.001	0.006	0.072	0.239	0.071	0.006	0.001	0.011	663.1 ± 4.1
17	610	–	0.001	0.006	0.071	0.228	0.069	0.006	0.001	0.011	668.3 ± 4.1
18	630	–	0.001	0.006	0.070	0.222	0.067	0.006	0.001	0.011	650.9 ± 4.0
19	650	–	0.001	0.006	0.067	0.210	0.064	0.005	–	0.011	628.8 ± 4.0
20	670	–	0.001	0.006	0.065	0.204	0.059	0.004	–	0.011	595.8 ± 4.0
21	690	–	0.001	0.006	0.063	0.195	0.055	0.003	–	0.011	544.5 ± 3.8
22	710	–	0.001	0.005	0.060	0.187	0.053	0.003	–	0.012	472.5 ± 3.7
23	730	–	–	0.005	0.055	0.179	0.052	0.002	–	0.012	380.7 ± 3.5
24	750	–	–	0.003	0.050	0.169	0.049	0.002	–	0.013	287.2 ± 2.9
25	770	–	–	0.003	0.045	0.165	0.042	0.001	–	0.014	181.0 ± 2.2
26	790	–	–	0.002	0.035	0.154	0.034	–	–	0.017	90.1 ± 1.6
27	810	–	–	0.001	0.026	0.142	0.027	–	–	0.024	32.3 ± 0.9
28	830	–	–	–	0.021	0.113	0.034	–	–	0.039	11.5 ± 0.6
29	850	–	–	–	0.010	0.075	–	–	–	1.004	3.4 ± 0.4
30	870	–	–	–	0.001	0.045	–	–	–	1.023	0.10 ± 0.06

TABLE II. The normalized $\pi^+\pi^-$ invariant mass spectrum. $H^{(0)}_i$ - the relative fraction of events with $\pi^+\pi^-$ invariant mass $m_i \pm 10$ MeV, efficiency matrix $b^{(0)}_{ij} = a^{(0)}_{ij} \cdot \epsilon^{(0)}_j$ and relative uncertainty $\delta P^{(\pm)}_i$ of the theoretical $\pi^+\pi^-$ mass distribution are also given.

i	m_i (MeV)	$b^{(\pm)}_{i,i-4}$	$b^{(\pm)}_{i,i-3}$	$b^{(\pm)}_{i,i-2}$	$b^{(\pm)}_{i,i-1}$	$b^{(\pm)}_{i,i}$	$b^{(\pm)}_{i,i+1}$	$b^{(\pm)}_{i,i+2}$	$b^{(\pm)}_{i,i+3}$	$b^{(\pm)}_{i,i+4}$	$\delta P^{(\pm)}_i$	$H^{(\pm)}_i \cdot 10^4$
1	290	–	–	–	–	0.030	0.006	–	–	–	1.004	2.1 ± 0.3
2	310	–	–	–	0.004	0.081	0.019	–	–	–	1.001	12.2 ± 0.7
3	330	–	–	–	0.015	0.119	0.033	0.001	–	–	0.021	33.8 ± 1.1
4	350	–	0.001	0.001	0.020	0.143	0.046	0.002	–	–	0.016	62.0 ± 1.3
5	370	–	–	0.001	0.033	0.162	0.059	0.004	–	–	0.013	102.0 ± 1.7
6	390	0.001	–	0.002	0.039	0.171	0.064	0.005	–	–	0.011	144.9 ± 1.9
7	410	–	–	0.002	0.048	0.177	0.071	0.006	–	–	0.010	194.4 ± 2.3
8	430	–	–	0.002	0.056	0.183	0.077	0.008	0.001	–	0.009	244.5 ± 2.6
9	450	–	–	0.004	0.062	0.185	0.079	0.010	0.001	–	0.008	298.5 ± 2.8
10	470	–	–	0.005	0.067	0.190	0.085	0.011	0.001	–	0.007	355.6 ± 3.0
11	490	–	0.001	0.007	0.068	0.185	0.087	0.013	0.001	0.001	0.007	417.9 ± 3.3
12	510	–	–	0.008	0.074	0.189	0.088	0.014	0.002	0.001	0.006	474.7 ± 3.5
13	530	–	–	0.010	0.075	0.186	0.091	0.017	0.003	0.001	0.006	526.1 ± 3.7
14	550	–	0.001	0.010	0.076	0.183	0.090	0.017	0.003	0.001	0.006	578.1 ± 3.9
15	570	–	0.001	0.013	0.078	0.177	0.093	0.017	0.003	0.001	0.006	620.4 ± 4.0
16	590	–	0.001	0.013	0.081	0.174	0.094	0.019	0.004	0.001	0.006	645.8 ± 4.1
17	610	–	0.002	0.015	0.079	0.170	0.094	0.019	0.004	0.001	0.006	667.3 ± 4.1
18	630	–	0.002	0.015	0.079	0.168	0.091	0.020	0.005	0.001	0.006	676.0 ± 4.1
19	650	0.001	0.003	0.016	0.080	0.166	0.090	0.020	0.005	0.001	0.006	673.4 ± 4.1
20	670	0.001	0.003	0.016	0.078	0.163	0.089	0.021	0.004	0.001	0.006	660.6 ± 4.1
21	690	0.001	0.003	0.017	0.078	0.163	0.090	0.023	0.005	0.001	0.006	631.5 ± 4.0
22	710	0.001	0.003	0.016	0.078	0.162	0.093	0.021	0.005	0.001	0.006	570.7 ± 3.8
23	730	0.001	0.004	0.017	0.078	0.163	0.090	0.022	0.005	0.001	0.007	498.4 ± 3.5
24	750	0.001	0.004	0.017	0.077	0.166	0.094	0.023	0.004	0.001	0.008	381.2 ± 3.0
25	770	0.001	0.003	0.017	0.077	0.160	0.091	0.020	0.002	–	0.010	259.5 ± 2.5
26	790	0.001	0.004	0.017	0.076	0.171	0.096	0.018	0.002	–	0.012	147.6 ± 1.9
27	810	0.001	0.003	0.016	0.073	0.167	0.087	0.014	–	–	0.018	72.6 ± 1.3
28	830	0.001	0.003	0.013	0.070	0.170	0.054	–	–	–	0.029	30.8 ± 0.9
29	850	0.001	0.002	0.013	0.060	0.171	0.029	–	–	–	1.001	11.7 ± 0.5
30	870	0.001	0.001	0.012	0.045	0.057	–	–	–	–	1.005	5.6 ± 0.4

TABLE III. The normalized $\pi^{\pm}\pi^0$ invariant mass spectrum. $H^{(\pm)}_i$ - the relative fraction of events with $\pi^{\pm}\pi^0$ invariant mass $m_i \pm 10$ MeV, efficiency matrix $b^{(\pm)}_{ij} = a^{(\pm)}_{ij} \cdot \epsilon^{(\pm)}_j$ and relative uncertainty $\delta P^{(\pm)}_i$ of the theoretical $\pi^{\pm}\pi^0$ mass distribution are also given.

N	1	2	3	4
$m_{\rho^0} - 770$ (MeV)	6.1±1.0	6.1±1.0	4.9±1.4	7.8±1.6
Γ_{ρ^0}(MeV)	151.1±2.6	150.7±3.5	156.0±4.0	151.2±2.6
$m_{\rho^\pm} - m_{\rho^0}$ (MeV)	-1.7±1.2	-1.8±1.2	-0.6±1.6	-1.9±1.2
$\Gamma_{\rho^\pm}$(MeV)	149.9±2.3	149.5±3.4	149.4±2.3	150.2±2.3
$\mathrm{Re}(a_{3\pi}) \cdot 10^5 (\mathrm{MeV})^{-2}$	0	0.04±0.25	0	0
$K_{\omega\pi/\rho\pi}$	0	0	0.3±0.1	0
$\phi_{\omega\pi/\rho\pi}$	0	0	-90.0±18.0	0
s_1	0	0	0	0.3±0.3
χ^2_0	27.1	26.9	19.0	25.0
$\chi^2_\pm$	28.9	29.1	29.5	29.6
χ^2/N_{df}	56.0/54	56.0/53	48.5/52	54.6/53

TABLE IV. Fit results for the $\pi^+\pi^-$ and $\pi^{\pm}\pi^0$ mass spectra.

N	1	2	3	4
$m_{\rho^0} - 770$ (MeV)	5.8±0.9	5.8±1.0	4.3±1.3	7.3±1.3
Γ_{ρ^0}(MeV)	149.9±2.2	149.5±3.1	149.3±2.3	149.9±2.2
$m_{\rho^\pm} - m_{\rho^0}$(MeV)	-1.3±1.1	-1.3±1.1	0.3±1.5	-1.4± 1.1
$\mathrm{Re}(a_{3\pi}) \cdot 10^5 (\mathrm{MeV})^{-2}$	0	0.04±0.24	0	0
$K_{\omega\pi/\rho\pi}$	0	0	0.2±0.1	0
$\phi_{\omega\pi/\rho\pi}$	0	0	-125.0±26.0	0
s_1	0	0	0	0.3±0.3
χ^2_0	26.9	26.8	24.0	24.9
$\chi^2_\pm$	29.9	30.0	30.0	30.7
χ^2/N_{df}	56.8/55	56.8/54	54.3/53	55.6/54

TABLE V. Fit results for the $\pi^+\pi^-$ and $\pi^\pm\pi^0$ mass spectra under assumption $g_{\rho^0\pi\pi} = g_{\rho^\pm\pi\pi}$.

N	1	2	3	4
$m_{\rho^0} - 770$ (MeV)	5.0±0.6	5.0±0.7	4.5±0.7	6.4±1.4
Γ_{ρ^0}(MeV)	149.8±2.2	149.7±3.1	149.3±2.3	149.9±2.2
$\mathrm{Re}(a_{3\pi}) \cdot 10^5 (\mathrm{MeV})^{-2}$	0	0.01±0.23	0	0
$K_{\omega\pi/\rho\pi}$	0	0	0.2±0.1	0
$\phi_{\omega\pi/\rho\pi}$	0	0	-125.0±28.0	0
s_1	0	0	0	0.3±0.3
χ^2_0	28.2	28.0	24.0	26.2
$\chi^2_\pm$	30.0	30.0	30.0	30.8
χ^2/N_{df}	58.2/56	58.0/55	58.0/54	57.1/55

TABLE VI. Fit results for the $\pi^+\pi^-$ and $\pi^\pm\pi^0$ mass spectra, under assumptions $g_{\rho^0\pi\pi} = g_{\rho^\pm\pi\pi}$ and $m_{\rho^0} = m_{\rho^\pm}$.

	m_{ρ^0}(MeV)	$m_{\rho^\pm}$(MeV)	$m_{\rho^\pm} - m_{\rho^0}$(MeV)
SND	$775.8 \pm 0.9 \pm 2.0$	$774.5 \pm 0.7 \pm 1.5$	$-1.3 \pm 1.1 \pm 2.0$
SND*	$775.0 \pm 0.6 \pm 1.1$	$775.0 \pm 0.6 \pm 1.1$	
CMD-2[19]	$775.3 \pm 0.6 \pm 0.2$		
ALEPH[20]		$776.4 \pm 0.9 \pm 1.5$	0.0 ± 1.0
CLEO[21]		$774.9 \pm 0.5 \pm 0.9$	
CBAR[22]	$762.3 \pm 0.5 \pm 1.2$	$763.0 \pm 0.3 \pm 1.3$	$-1.6 \pm 0.6 \pm 1.7$
PDG-1[12]	776.0 ± 0.9	776.0 ± 0.9	
PDG-2[12]	769.3 ± 0.8	769.3 ± 0.8	-0.4 ± 0.8
	Γ_{ρ^0}(MeV)	$\Gamma_{\rho^\pm}$(MeV)	$a_{3\pi} \times 10^5$(MeV)$^{-2}$
SND	$151.1 \pm 2.6 \pm 3.0$	$149.9 \pm 2.3 \pm 2.0$	
SND**	$149.8 \pm 2.2 \pm 2.0$	$150.9 \pm 2.2 \pm 2.0$	$0.01 \pm 0.23 \pm 0.25$
CMD-2[19,6]	$147.7 \pm 1.3 \pm 0.4$		$0.08 \pm 0.45 \pm 0.37$
ALEPH[20]		$150.5 \pm 1.6 \pm 6.3$	
CLEO[21]		$149.0 \pm 1.1 \pm 0.7$	
CBAR[22]	147.0 ± 2.5	149.5 ± 1.3	
PDG-1[12]	150.5 ± 2.7	150.5 ± 2.7	
PDG-2[12]	150.2 ± 0.8	150.2 ± 0.8	
	$K_{\omega\pi/\rho\pi}$	$\phi_{\omega\pi/\rho\pi}$	s_1
SND	$0.20 \pm 0.10 \pm 0.05$	$-125^\circ \pm 28^\circ$	$0.3 \pm 0.3 \pm 0.3$

TABLE VII. Comparison of the results of various experiments. SND – this work; SND* – the ρ meson mass from our fit under $m_{\rho^0} = m_{\rho^\pm}$ assumption; SND** – the ρ^0 and $\rho^\pm$ widths from our fit under $g_{\rho^0\pi\pi} = g_{\rho^\pm\pi\pi}$ assumption; PDG-1 – the world average values of e^+e^- annihilation and τ decay experiments only; PDG-2 – the world average values for all experiments.

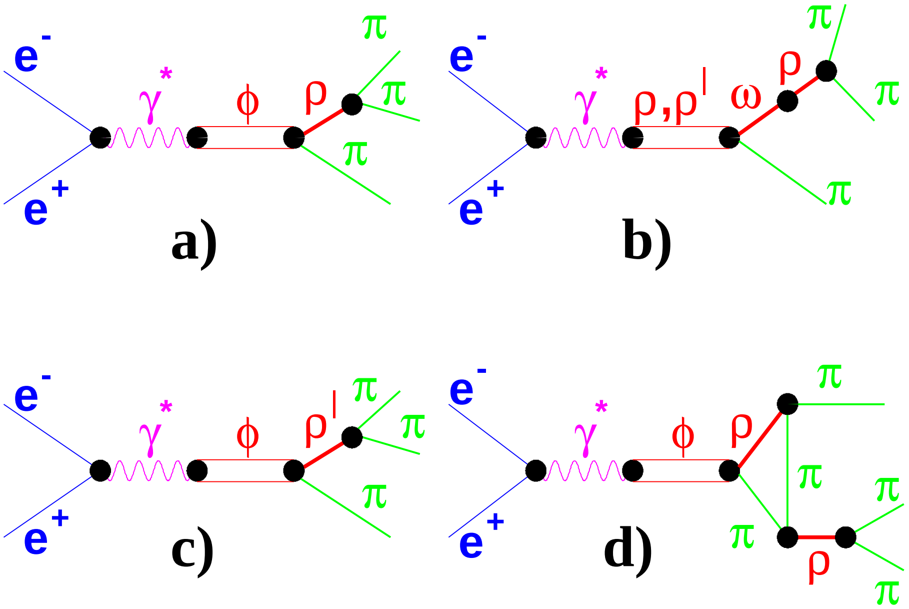

FIG. 1. $e^+e^- \to \phi \to \rho\pi \to \pi^+\pi^-\pi^0$ transition diagrams. a), b), c) – through various intermediate states. d) – the $e^+e^- \to \phi \to \rho\pi \to \pi^+\pi^-\pi^0$ transition with ρ and π mesons interaction in the final state.

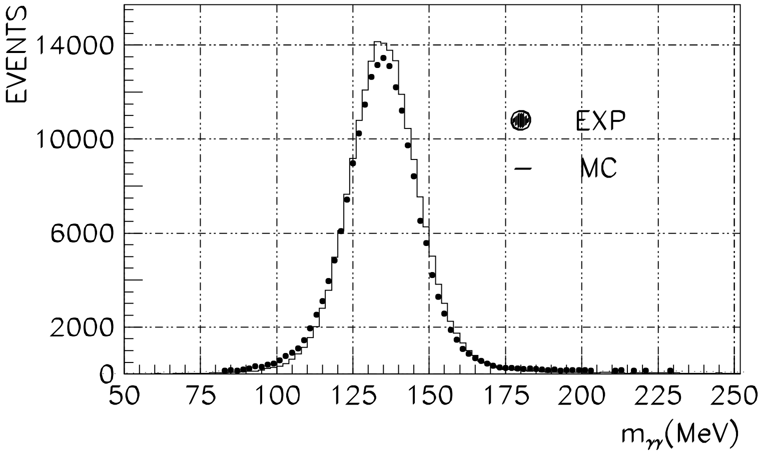

FIG. 2. Two-photon invariant mass distribution in the $e^+e^- \to \pi^+\pi^-\pi^0$ events.

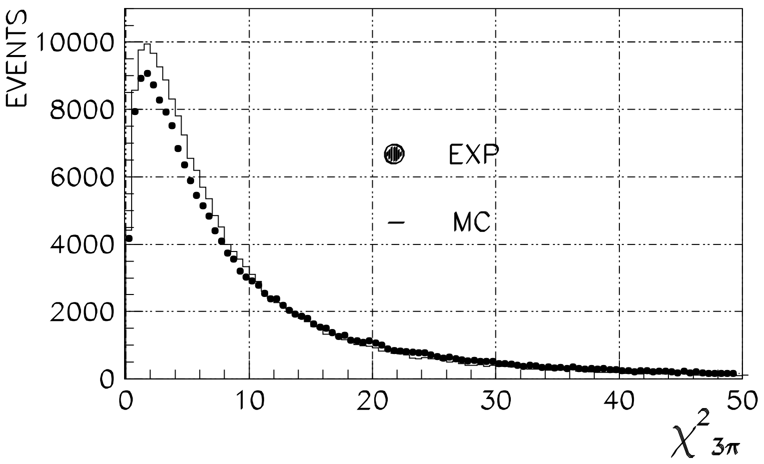

FIG. 3. The $\chi^2_{3\pi}$ distribution in $e^+e^- \to \pi^+\pi^-\pi^0$ events.

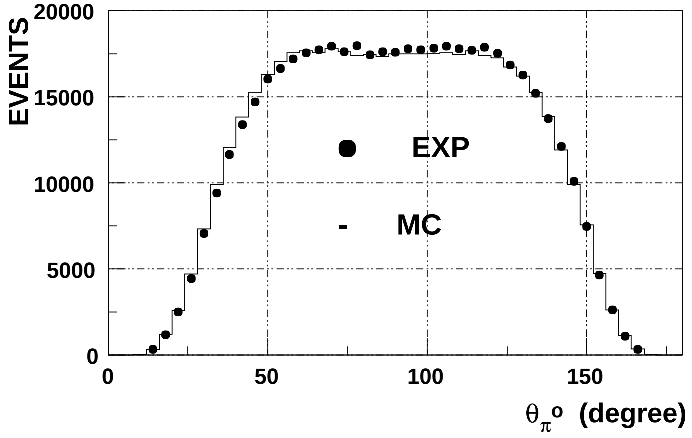

FIG. 4. The θ distribution of neutral pions from the reaction $e^+e^- \to \pi^+\pi^-\pi^0$.

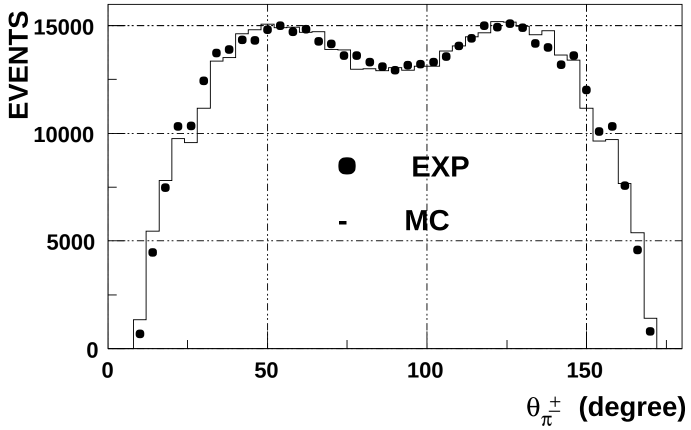

FIG. 5. The θ distribution of charged pions from the reaction $e^+e^- \to \pi^+\pi^-\pi^0$.

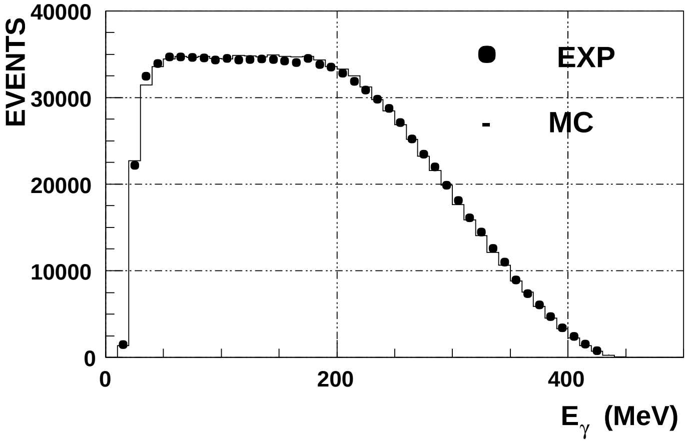

FIG. 6. Photons energy distribution.

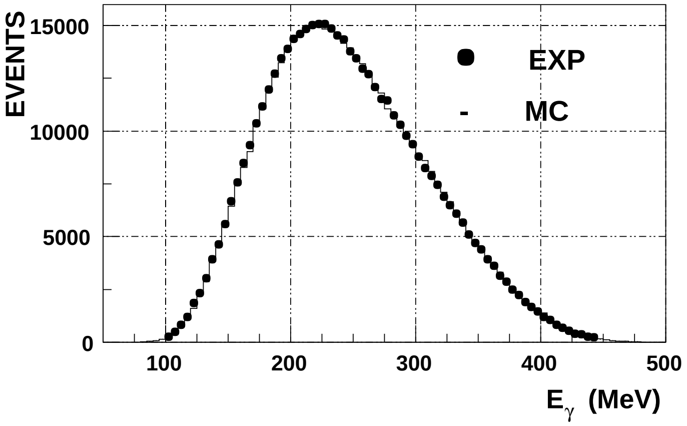

FIG. 7. The maximal photon energy distribution.

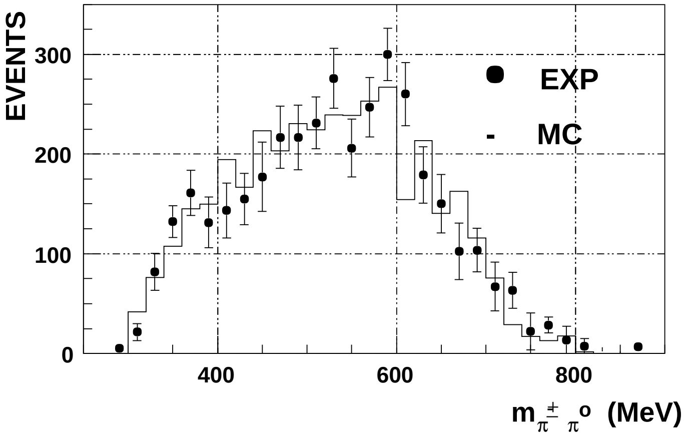

FIG. 8. "$\pi^{\pm}\pi^{0}$" mass distribution from $e^{+}e^{-} \rightarrow K_{S}K_{L}$ background events.

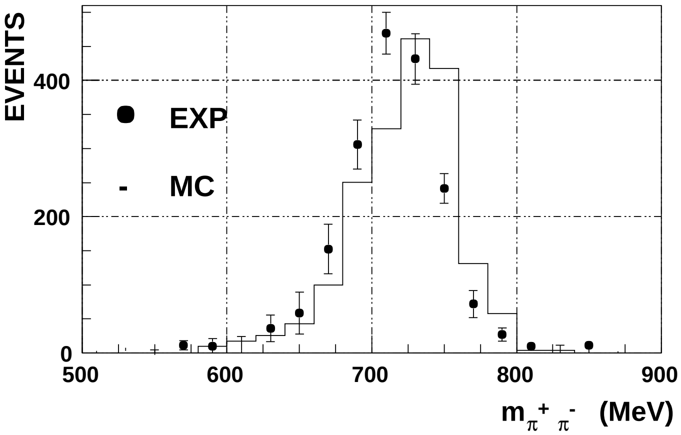

FIG. 9. "$\pi^+\pi^-$" mass distribution from the $e^+e^- \to K_S K_L$ background events.

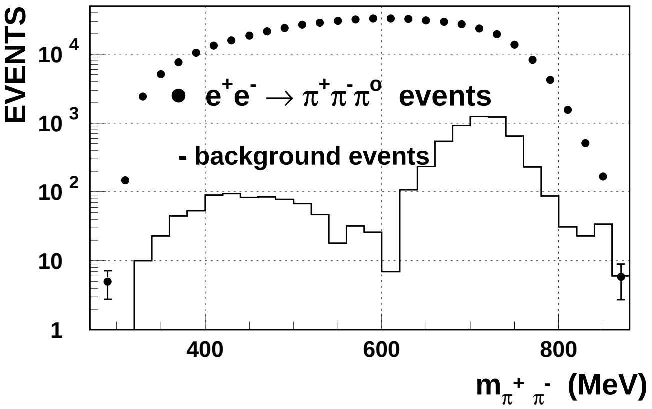

FIG. 10. $\pi^+\pi^-$ mass distribution for selected $e^+e^- \to \pi^+\pi^-\pi^0$ events and background contribution

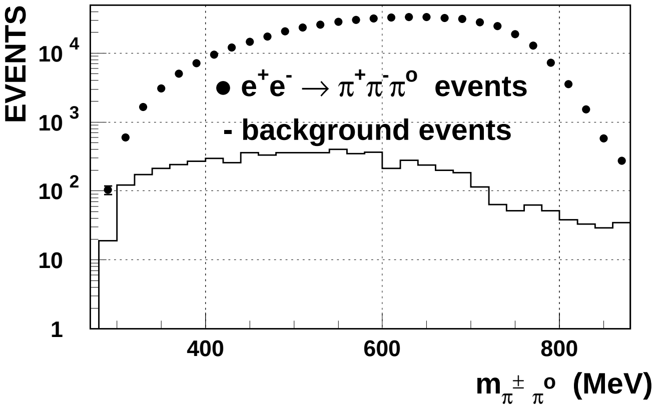

FIG. 11. $\pi^\pm\pi^0$ mass distribution for selected $e^+e^- \to \pi^+\pi^-\pi^0$ events and background contribution

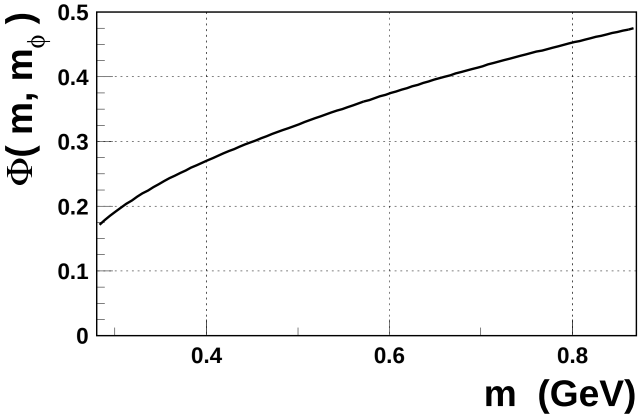

FIG. 12. $\Phi(m, s)$ as the function of the dipion mass m at $\sqrt{s} = m_\phi$

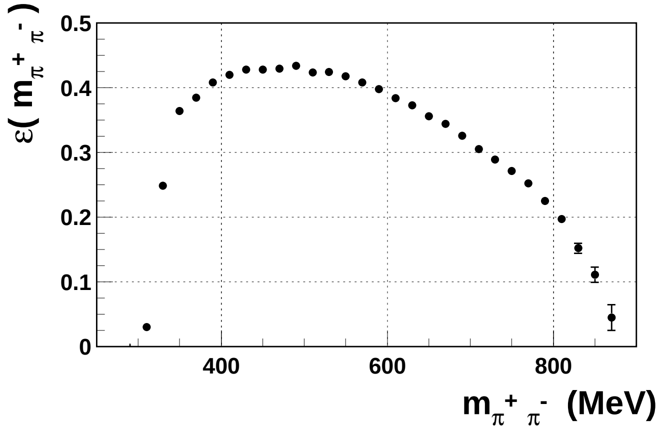

FIG. 13. Detection efficiency for $\pi^+\pi^-$ mass spectrum.

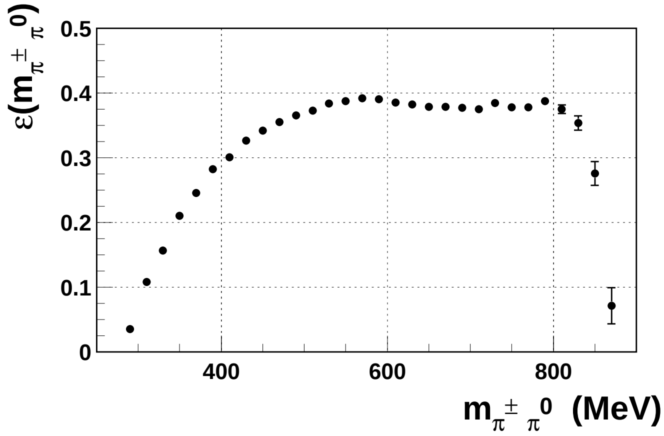

FIG. 14. Detection efficiency for $\pi^\pm\pi^0$ mass spectrum.

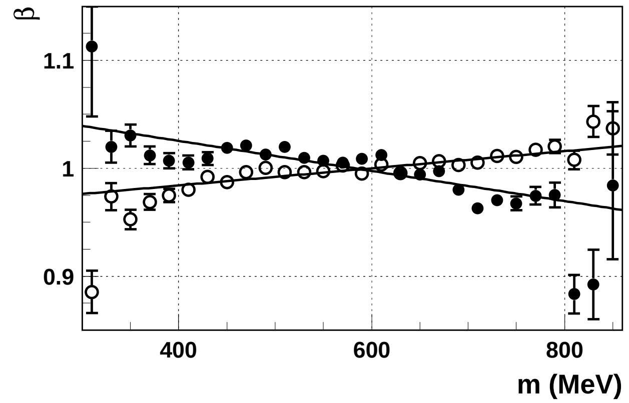

FIG. 15. The correction coefficients $\beta^{(0)}$ and $\beta^{(\pm)}$ upto irrelevant normalization factor. Dots - $\beta^{(0)}$ correction coefficient to the detection efficiency for $\pi^+\pi^-$ mass spectrum. Circles – $\beta^{(\pm)}$ correction coefficient to the detection efficiency for $\pi^\pm\pi^0$ mass spectrum

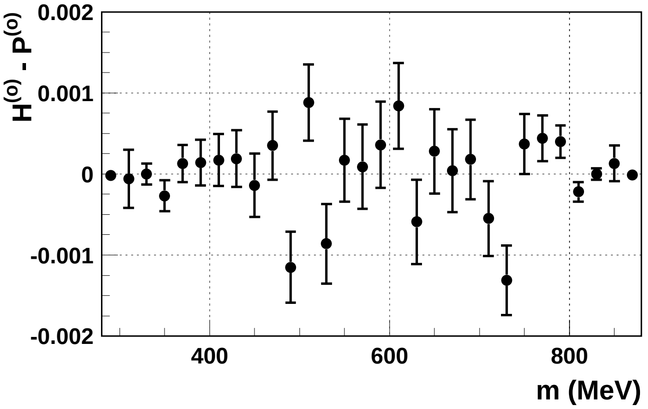

FIG. 16. The difference between the experimental and theoretical $m_{\pi^+\pi^-}$ spectra.

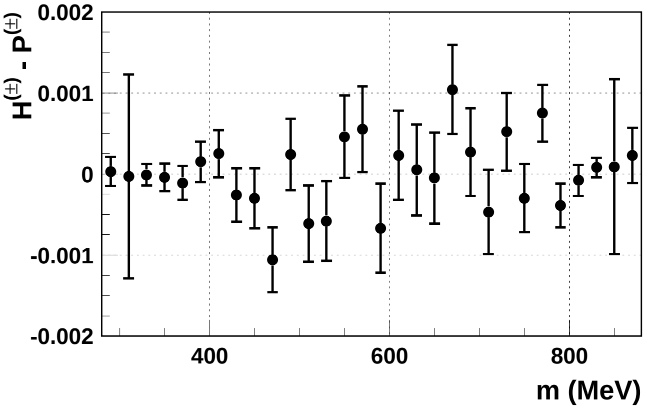

FIG. 17. The difference between the experimental and theoretical $m_{\pi^\pm\pi^0}$ spectra.

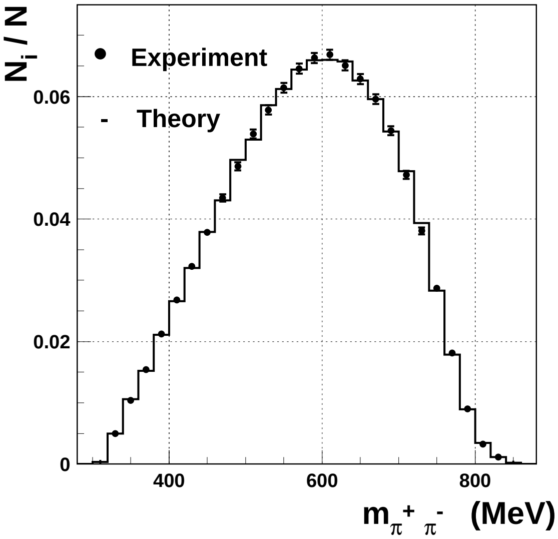

FIG. 18. The fit result for the $\pi^+\pi^-$ mass spectrum.

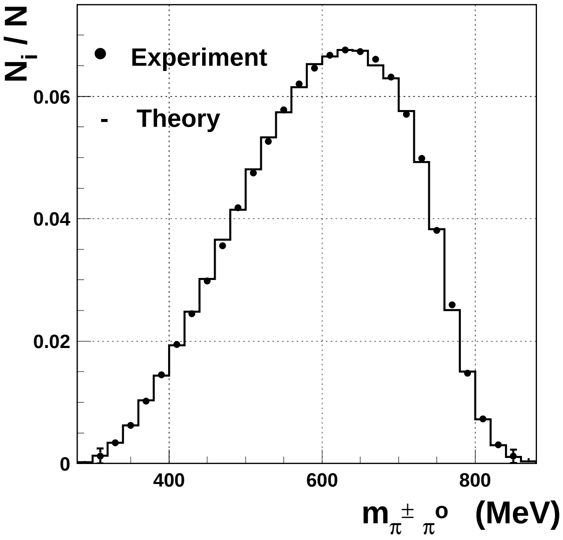

FIG. 19. The fit result for the $\pi^\pm\pi^0$ mass spectrum.